Casimir Interaction between Plane and Spherical Metallic Surfaces

Antoine Canaguier-Durand,[1] Paulo A. Maia Neto,[2] Ines Cavero-Pelaez,[1] Astrid Lambrecht,[1] and Serge Reynaud[1]

[1]*Laboratoire Kastler Brossel, CNRS, ENS, Université Pierre et Marie Curie case 74, Campus Jussieu, F-75252 Paris Cedex 05, France*
[2]*Instituto de Física, UFRJ, CP 68528, Rio de Janeiro, RJ, 21941-972, Brazil*
(Received 17 January 2009; published 11 June 2009)

We give an exact series expansion of the Casimir force between plane and spherical metallic surfaces in the nontrivial situation where the sphere radius R, the plane-sphere distance L and the plasma wavelength λ_P have arbitrary relative values. We then present numerical evaluation of this expansion for not too small values of L/R. For metallic nanospheres where R, L and λ_P have comparable values, we interpret our results in terms of a correlation between the effects of geometry beyond the proximity force approximation and of finite reflectivity due to material properties. We also discuss the interest of our results for the current Casimir experiments which are performed with spheres of large radius $R \gg L$.

The Casimir force is a striking macroscopic effect of quantum vacuum fluctuations which has been seen in a number of dedicated experiments in the last decade (see for example [1,2] and references therein). One aim of the Casimir force experiments is to investigate the presence of hypothetical weak forces predicted by unification models through a careful comparison of the measurements with quantum electrodynamics predictions. This aim can only be reached if theoretical computations are able to take into account a realistic and reliable modeling of the experimental conditions. Among the effects to be taken into account are the material properties and the surface geometry. Note that these effects are also able to produce phenomena of interest in nanosystems [3,4].

A number of Casimir measurements have been performed with gold-covered plane and spherical surfaces separated by distances L of the order of the plasma wavelength ($\lambda_P \simeq 136$ nm for gold), making material properties important in their analysis [5]. As those measurements use spheres with a radius $R \gg L$, they are commonly analyzed through the proximity force approximation (PFA) [6], which amounts to a trivial integration over the sphere-plate distances. An exception is the Purdue experiment dedicated to the investigation of the accuracy of PFA in the sphere-plate geometry [7], the result of which will be given as a precise statement below.

In the present Letter, we give for the first time an exact series expansion of the Casimir force between a plane and a sphere in an electromagnetic vacuum, taking into account the material properties via the plasma model (see Fig. 1). We present numerical evaluation of this expansion which are limited to not too small values of L/R, because of the multipolar nature of the series. We show below that these new results lead to a striking correlation between the effects of geometry and imperfect reflection when evaluated for nanospheres, with R, L, and λ_P having comparable values. In the end of this Letter, we also discuss the interest of these results for the Casimir experiments performed with large spheres $R \gg L$ [7].

Our starting point is a general scattering formula for the Casimir energy [8]. Using suitable plane-wave and multipole bases, we deduce the Casimir energy $\mathcal{E}_{\mathrm{PS}}$ between a plane and a spherical metallic surface in an electromagnetic vacuum. The multipole series expansion is written in terms of Fresnel reflection amplitudes for the plate and Mie coefficients for the sphere, and it is valid for arbitrary relative values of the sphere radius R, the sphere-plate distance L and the plasma wavelength λ_P. For the sake of comparison with experiments, we assume $\lambda_P \simeq 136$ nm for both, the sphere and the plate. We occasionally also consider the limit $\lambda_P \to 0$, where the formula reduces to the case of perfect reflectors in an electromagnetic vacuum, for which results were obtained recently [9–11].

In the following, we discuss the force $\mathcal{F}_{\mathrm{PS}} \equiv -\partial \mathcal{E}_{\mathrm{PS}}/\partial L$ as well as the force gradient $\mathcal{G}_{\mathrm{PS}} \equiv -\partial \mathcal{F}_{\mathrm{PS}}/\partial L$ which was measured in the experiment [7]. We write the results deduced from the scattering formula as products of PFA estimates by beyond-PFA correction factors ρ_F and ρ_G:

$$\mathcal{F}_{\mathrm{PS}} \equiv \rho_F \mathcal{F}_{\mathrm{PS}}^{\mathrm{PFA}}, \qquad \mathcal{F}_{\mathrm{PS}}^{\mathrm{PFA}} \equiv \eta_E \frac{\hbar c \pi^3 R}{360 L^3}$$
$$\mathcal{G}_{\mathrm{PS}} \equiv \rho_G \mathcal{G}_{\mathrm{PS}}^{\mathrm{PFA}}, \qquad \mathcal{G}_{\mathrm{PS}}^{\mathrm{PFA}} \equiv \eta_F \frac{\hbar c \pi^3 R}{120 L^4}.$$
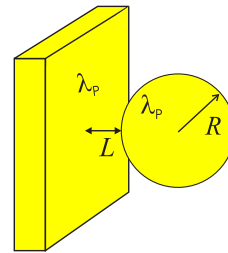
(1)

FIG. 1 (color online). The geometry of a sphere of radius R and a flat plate at a distance L (center-to-plate distance $\mathcal{L} \equiv L + R$); both mirrors are covered with a metal characterized by a plasma wavelength λ_P.

The PFA estimates $\mathcal{F}_{PS}^{PFA}$ and $\mathcal{G}_{PS}^{PFA}$ are proportional, respectively, to the energy and force calculated between two planes. They are written as products of ideal Casimir expressions and factors η_E and η_F accounting for the effect of imperfect reflection [5].

The beyond-PFA correction factors ρ_F and ρ_G appearing in (1) are the important quantities for what follows. For experiments performed with large spheres of radius $R \gg L$, the deviation from PFA is small ($\rho_F \simeq 1$). Even in this limit, it remains important to specify the accuracy of PFA in order to master the quality of theory-experiment comparison [10]. This can be done by introducing a Taylor expansion of the correction factors at small values of L/R

$$\rho_{F,G} \equiv 1 + \beta_{F,G}\frac{L}{R} + O\left(\frac{L^2}{R^2}\right). \qquad (2)$$

The only experimental result available on this topic [7] may be stated as a bound on the β_G factor, namely $|\beta_G| < 0.4$. On the theoretical side, analytical as well as numerical calculations of this slope have been obtained for scalar field models [12–16]. For the situation met in experiments, with a plane and a sphere in an electromagnetic vacuum, an estimation technique has recently been proposed where the slope is deduced from a polynomial fit of the numerical values obtained at intermediate values of L/R [9,10]. The slope obtained in this manner is much larger (~ 8 times larger) than expected from scalar field models [10]. As a consequence, the value of β_G falls out of the bound of [7], in contrast with the scalar prediction which lies within the bound. More precise statements on this point will be given below.

On the other hand all these results correspond to perfect reflection, whereas the experiment [7] was performed with gold-covered surfaces. The apparent contradiction noticed in the preceding paragraph may thus be cured if the value of β_G differs for metallic and perfect mirrors, that is also if the effects of geometry and finite reflectivity are correlated. We show in the sequel of this Letter that this is indeed the case.

We start from the formula for the Casimir energy $\mathcal{E}_{PS}$ between two scatterers in vacuum [8]

$$\mathcal{E}_{PS} = \hbar \int_0^\infty \frac{d\xi}{2\pi} \log\det(1 - \mathcal{M})$$
$$\mathcal{M} \equiv \mathcal{R}_S e^{-\mathcal{K}\mathcal{L}} \mathcal{R}_P e^{-\mathcal{K}\mathcal{L}}. \qquad (3)$$

In the geometry depicted on Fig. 1 with a sphere of radius R, a plate, and a sphere-plate separation L along the z axis (center-to-plate distance $\mathcal{L} \equiv L + R$), $\mathcal{R}_S$ and $\mathcal{R}_P$ represent the reflection operators for the spherical and the plane scatterers, respectively. They are evaluated with reference points placed at the sphere center and at its projection on the plane, respectively. The operator $e^{-\mathcal{K}\mathcal{L}}$ describes the one-way propagation between these two reference points. ξ is the imaginary field frequency integrated over the upper imaginary axis.

In order to evaluate explicitly this expression, we use two mode decompositions. The first one is a plane-wave basis $|\mathbf{k}, \phi, p\rangle_\xi$ with $\mathbf{k}$ the transverse wave vector parallel to the xy plane, $p = \text{TE}, \text{TM}$ the polarization, and $\phi = \pm 1$ for rightward or leftward propagation directions. It is well adapted to the description of free propagation and reflection on the plane: the propagation operator $e^{-\mathcal{K}\mathcal{L}}$ is diagonal with matrix elements $e^{-K\mathcal{L}}$ such that $K = \sqrt{\xi^2/c^2 + k^2}$ ($k \equiv |\mathbf{k}|$) while reflection on the plane preserves all plane-wave quantum numbers but ϕ. The nonzero elements of $\mathcal{R}_P$ are the standard Fresnel reflection amplitudes r_p. Given values of $\mathbf{k}(k, \varphi)$ and $\phi = \pm 1$ define a direction in reciprocal space corresponding to the azimuthal angle φ and a complex angle $\theta^\pm$ such that $\sin\theta^\pm = -i\frac{ck}{\xi}$ and $\cos\theta^\pm = \pm\frac{cK}{\xi}$.

The second basis, which is adapted to the spherical symmetry of $\mathcal{R}_S$, is a multipole basis $|\ell m P\rangle_\xi$, with $\ell(\ell + 1)$ and m the angular momentum eigenvalues ($\ell = 1, 2, \ldots$, $m = -\ell, \ldots, \ell$) and $P = E, M$ for the electric and magnetic multipoles. By rotational symmetry around the z axis, $\mathcal{M}$ commutes with J_z. Hence it is block diagonal, with each block $\mathcal{M}^{(m)}$ corresponding to a common value of m and yielding a contribution $\mathcal{E}_{PS}^{(m)}$ to the Casimir energy $\mathcal{E}_{PS}$ (opposite values $\pm m$ provide identical contributions). The contribution $\mathcal{E}_{PS}^{(m)}$ is written as in (3) with $\mathcal{M}$ replaced by the block matrix

$$\mathcal{M}^{(m)} = \begin{pmatrix} M^{(m)}(E, E) & M^{(m)}(E, M) \\ M^{(m)}(M, E) & M^{(m)}(M, M) \end{pmatrix}. \qquad (4)$$

Each block in this matrix is the sum of TE and TM contributions $M^{(m)}(P_1, P_2) = \sum_p M_p^{(m)}(P_1, P_2)$. The diagonal blocks are written as

$$M_{TE}^{(m)}(E, E)_{\ell_1, \ell_2} = \sqrt{\frac{\pi(2\ell_1 + 1)}{\ell_2(\ell_2 + 1)}} A_{\ell_1, \ell_2, TE}^{(m)} a_{\ell_1}(i\xi)$$

$$M_{TM}^{(m)}(E, E)_{\ell_1, \ell_2} = \sqrt{\frac{\pi(2\ell_1 + 1)}{\ell_2(\ell_2 + 1)}} B_{\ell_1, \ell_2, TM}^{(m)} a_{\ell_1}(i\xi)$$

$$M_{TM}^{(m)}(M, M)_{\ell_1, \ell_2} = \sqrt{\frac{\pi(2\ell_1 + 1)}{\ell_2(\ell_2 + 1)}} A_{\ell_1, \ell_2, TM}^{(m)} b_{\ell_1}(i\xi)$$

$$M_{TE}^{(m)}(M, M)_{\ell_1, \ell_2} = \sqrt{\frac{\pi(2\ell_1 + 1)}{\ell_2(\ell_2 + 1)}} B_{\ell_1, \ell_2, TE}^{(m)} b_{\ell_1}(i\xi), \qquad (5)$$

$a_\ell(i\xi)$ and $b_\ell(i\xi)$ are the Mie coefficients [17] for electric and magnetic multipoles. A and B are matrices which do not depend on the radius nor on the refractive index of the sphere and are written in terms of the spherical harmonics $Y_{\ell,m}(\theta, \varphi = 0)$ and the finite rotation matrix elements $d_{m,m'}^\ell(\theta) = \langle \ell, m|e^{-i\theta J_y}|\ell, m'\rangle$ [18]

$$
\begin{aligned}
A^{(m)}_{\ell_1,\ell_2,p} &= -im \int_0^\infty \frac{dk}{K} (d^{\ell_1}_{m,1}(\theta^+) + d^{\ell_1}_{m,-1}(\theta^+)) \\
&\quad \times Y_{\ell_2 m}(\theta^-) r_p(k) e^{-2K\mathcal{L}} \\
B^{(m)}_{\ell_1,\ell_2,p} &= -\frac{c}{\xi} \int_0^\infty \frac{kdk}{K} (d^{\ell_1}_{m,1}(\theta^+) - d^{\ell_1}_{m,-1}(\theta^+)) \\
&\quad \times \partial_\theta Y_{\ell_2 m}(\theta^-) r_p(k) e^{-2K\mathcal{L}}.
\end{aligned}
\tag{6}
$$

Similar expressions are found for the nondiagonal blocks, with the matrices A and B replaced, respectively, by

$$
\begin{aligned}
C^{(m)}_{\ell_1,\ell_2,p} &= \frac{c}{\xi} \int_0^\infty \frac{kdk}{K} (d^{\ell_1}_{m,1}(\theta^+) + d^{\ell_1}_{m,-1}(\theta^+)) \\
&\quad \times \partial_\theta Y_{\ell_2 m}(\theta^-) r_p(k) e^{-2K\mathcal{L}} \\
D^{(m)}_{\ell_1,\ell_2,p} &= im \int_0^\infty \frac{dk}{K} (d^{\ell_1}_{m,1}(\theta^+) - d^{\ell_1}_{m,-1}(\theta^+)) \\
&\quad \times Y_{\ell_2 m}(\theta^-) r_p(k) e^{-2K\mathcal{L}}.
\end{aligned}
\tag{7}
$$

In order to go further, we assume the materials to have a dielectric response described by the plasma model $\epsilon(i\xi) = 1 + \omega_P^2/\xi^2$, with ω_P the plasma frequency and $\lambda_P = 2\pi c/\omega_P$ the plasma wavelength. Although the formalism easily allows for different values of λ_P for both surfaces, we take a common value as in the recent experiment [7]. We calculate the Casimir energy $\mathcal{E}_{PS}$ and deduce the force $\mathcal{F}_{PS}$ and gradient $\mathcal{G}_{PS}$, both quantities being functions of the 3 length scales R, L, and λ_P. The case of perfect reflection [10] can be recovered as the limit $\lambda_P \ll R$, L (see [19] for the opposite non-retarded limit). A large distance limit may also be taken as λ_P, $R \ll L$. Its result reduces to the Rayleigh expression [20] in the case ($R \ll \lambda_P$) or to $3/2$ of it [9,10] in the case ($\lambda_P \ll R$).

As already discussed, the PFA expression is also contained in our general result, and it is recovered asymptotically for $R \gg L$. In the following, we discuss the results of numerical computations of the ratios $\rho_{F,G}$ defined in (1) which measure the deviation from PFA. For dimensionality reasons $\rho_{F,G}$ are functions of two dimensionless parameters built upon L, R, and λ_P ($\eta_{E,F}$ are functions of L/λ_P only [5]) and they approach unity at the PFA limit $L/R \ll 1$. Their numerical computation is done after truncating the vector space at some maximum value ℓ_{max} of the orbital number ℓ. As a consequence of the "localization principle" [21], the results are accurate only for R/L smaller than some value which increases with ℓ_{max}. At the moment, our numerical calculations are limited to $\ell_{max} = 24$, allowing us to obtain accurate results down to $L/R \simeq 0.2$ but not in close vicinity of the PFA limit.

This method gives new and interesting results, in particular, for nanospheres having a radius R with the same order of magnitude as the plasma wavelength λ_P. In this case, we can perform accurate calculations for L having a comparable magnitude, and thus explore the rich functional dependence of $\rho_{F,G}$ versus two dimensionless parameters built up on L, R, and λ_P. Figure 2 shows the results obtained for ρ_F and ρ_G with metallic and perfect
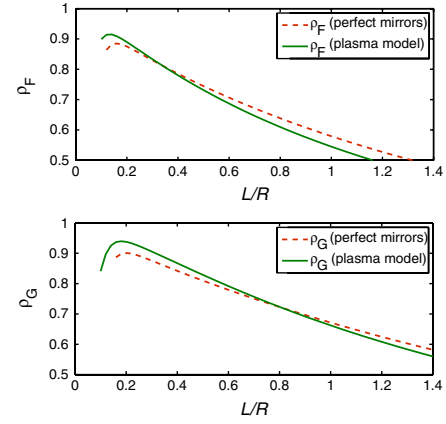

FIG. 2 (color online). Top graph: variation of ρ_F as a function of L/R, for a nanosphere of radius $R = 100$ nm; the solid green line corresponds to gold-covered plates ($\lambda_P = 136$ nm) and the dashed red line to perfect reflectors. Bottom graph: variation of ρ_G as a function of L/R, with the same conventions as in the top graph. The decreases at low values of L/R represent a numerical inaccuracy due to the limited value of $\ell_{max} = 24$.

mirrors. Clearly the deviation from the PFA calculated for metallic mirrors differs markedly from that already known for perfect mirrors. For small values of L/R the violation of PFA for the Casimir force and gradient turns out to be less pronounced for metallic mirrors than for perfect mirrors, while for large values of L/R it is more pronounced.

However, at values $L/R \simeq 0.2$ we find a clear correlation between geometry and finite reflectivity effects, therefore making measurements with nanospheres at small plate-sphere separations particularly interesting. This nontrivial interplay becomes evident when a polynomial fit of the numerical values of $\rho_{F,G}$ is used for inferring the behavior at small values of L/R [9,10]. In Fig. 3 we plot the quartic polynomial fits of the function ρ_G for the two cases of gold-covered and perfect mirrors. The curves were obtained by finding the best fit of the numerically computed
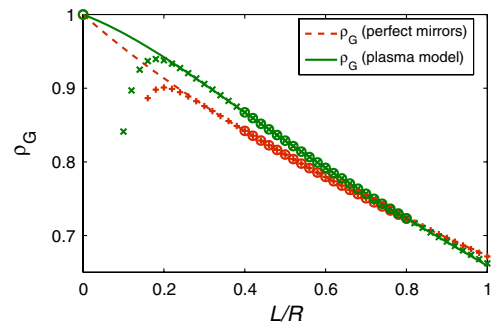

FIG. 3 (color online). Quartic polynomial fit of the function $\rho_G(L/R)$, for a nanosphere of radius $R = 100$ nm; the solid green line corresponds to gold-covered plates and the dashed red line to perfect reflectors. The crosses represent numerically evaluated points and the circles indicate those points which are used for the fit.

values of ρ_G (crosses on Fig. 3) in the window $0.4 < L/R < 0.8$ (circled crosses on Fig. 3) in the set of quartic polynomials (Taylor expansion defined as in (2) and truncated at fourth order). The left-hand bound of the window is fixed by the requirement of using only points accurately calculated with $\ell_{max} = 24$ while the right-hand bound is determined by the truncation at fourth order of the Taylor expansion. The best fits correspond to the following polynomials for gold-covered (GM) and perfect (PM) mirrors, respectively, ($x \equiv L/R$)

$$\text{GM}: 1 - 0.207x - 0.530x^2 + 0.645x^3 - 0.249x^4$$
$$\text{PM}: 1 - 0.483x + 0.297x^2 - 0.221x^3 + 0.080x^4. \tag{8}$$

The two fits are clearly different and this, in particular, is the case for the values obtained for the slope at $L/R = 0$. The slope ($\beta_G \sim -0.21$) obtained for gold mirrors differs by more than a factor 2 from the one ($\beta_G \sim -0.48$) obtained for perfect mirrors. This is related to the bending of the curve for gold mirrors at small L/R, which describes the effect of imperfect reflection in the beyond-PFA factor ρ_G and has to be contrasted with the unbent curve for perfect mirrors. For the same reason, we observe that the slope obtained for gold mirrors is less stable under the variation of the conditions of the best-fit procedure than that for perfect mirrors. To appreciate the meaning of the bending let us recall that the slope obtained for perfect mirrors in an electromagnetic vacuum is ~ 8 times larger than expected from scalar computations [15,16] and one cannot but notice that it lies outside the bound $|\beta_G| < 0.4$ of [7]. In contrast, the slope obtained for metallic mirrors lies within the bound. Let us emphasize that there is no contradiction between the results presented here (obtained for nanospheres with $R = 100$ nm) and the experiments (performed with spheres having $R >$ a few tenths of μm).

For spheres with large radii ($L/R > 0.2$) the beyond-PFA factors $\rho_{F,G}$ have the same values for gold-covered and perfect mirrors, because the value of L is much larger than λ_P. If we extracted a slope from these results, we would obtain a value close to that of perfect mirrors, thus lying outside the bound of [7]. However, the arguments discussed before show that one should refrain from doing so. Indeed, a bending of the curve has to be expected in this case too, for values of L becoming comparable to λ_P and thus much smaller than R. In contrast, this bending has no reason to appear for perfect mirrors since there is no length scale like λ_P in this case. If the bending is similar for large and small spheres, it may turn out that the slope for gold-covered mirrors meets the bound [7] while that for perfect mirrors does not.

To sum up our results, we have written a new and exact expansion for the Casimir force between plane and spherical metallic surfaces in an electromagnetic vacuum. The results go beyond the proximity force approximation, and show a clear correlation between the plane-sphere geometry and the material properties of the metallic surfaces. They constitute a new step in the direction of accurate

comparisons between Casimir experiments and QED theoretical predictions. More work is needed to obtain exact results for the Casimir force between a metallic sphere and plate in the so far experimentally explored parameter region of $L/R \simeq 0.01$, using, for example, different approaches based on semiclassical methods. Our results also indicate a complementary way to observe deviations from PFA and the interplay between geometrical and reflectivity effects in new experiments performed with nanospheres.

[1] R. Onofrio, New J. Phys. **8**, 237 (2006).
[2] R. Decca, D. Lopez, and E. Fischbach *et al.*, Phys. Rev. D **75**, 077101 (2007).
[3] H. B. Chan, Y. Bao, and J. Zou *et al.*, Phys. Rev. Lett. **101**, 030401 (2008).
[4] A. Lambrecht and V. N. Marachevsky, Phys. Rev. Lett. **101**, 160403 (2008).
[5] A. Lambrecht and S. Reynaud, Eur. Phys. J. D **8**, 309 (2000).
[6] B. V. Deriagin, I. I. Abrikosova, and E. M. Lifshitz, Quart. Rev. **10**, 295 (1968).
[7] D. E. Krause, R. S. Decca, D. Lopez, and E. Fischbach, Phys. Rev. Lett. **98**, 050403 (2007).
[8] A. Lambrecht, P. A. Maia Neto, and S. Reynaud, New J. Phys. **8**, 243 (2006).
[9] T. Emig and R. L. Jaffe, J. Phys. A **41**, 164001 (2008); T. Emig, J. Stat. Mech. (2008) P04007.
[10] P. A. Maia Neto, A. Lambrecht, and S. Reynaud, Phys. Rev. A **78**, 012115 (2008).
[11] O. Kenneth and I. Klich, Phys. Rev. B **78**, 014103 (2008).
[12] M. Schaden and L. Spruch, Phys. Rev. Lett. **84**, 459 (2000).
[13] H. Gies and K. Klingmüller, Phys. Rev. Lett. **96**, 220401 (2006).
[14] A. Scardicchio and R. L. Jaffe, Nucl. Phys. B **743**, 249 (2006).
[15] A. Wirzba, J. Phys. A **41**, 164003 (2008).
[16] M. Bordag and V. Nikolaev, J. Phys. A **41**, 164002 (2008).
[17] C. F. Bohren and D. R. Huffman, *Absorption and Scattering of Light by Small Particles* (Wiley, New York, 1983), Chap. 4.
[18] A. R. Edmonds, *Angular Momentum in Quantum Mechanics* (Princeton University Press, Princeton, 1957).
[19] C. Noguez, C. E. Román-Velázquez, R. Esquivel-Sirvent, and C. Villarreal, Europhys. Lett. **67**, 191 (2004).
[20] S. Y. Buhmann, D.-G. Welsch, and T. Kampf, Phys. Rev. A **72**, 032112 (2005).
[21] H. M. Nussenzveig, *Diffraction Effects in Semiclassical Scattering* (Cambridge University Press, Cambridge, England, 1992).